10B.5 VORTICITY-BASED DETECTION OF TROPICAL CYCLOGENESIS

Michelle M. Hite[1]*, Mark A. Bourassa[1,2], Philip Cunningham[2], James J. O'Brien[1,2], and Paul D. Reasor[2]
[1]Center for Ocean-Atmospheric Prediction Studies, Florida State University, Tallahassee, Florida
[2]Department of Meteorology, Florida State University, Tallahassee, Florida

1. INTRODUCTION

Tropical cyclogenesis (TCG), although an already well researched area, remains a highly debatable and unresolved topic. While considerable attention has been paid to tropical cyclone formation, little attention has focused on observational studies of the very early stages of TCG, otherwise referred to as the genesis stage. In the past, the early stages of TCG were unverifiable in surface observations, due to the paucity of meteorological data over the tropical oceans. The advent of wide swath scatterometers helped alleviate this issue by affording the scientific community with widespread observational surface data across the tropical basins. One such instrument is the SeaWinds scatterometer, aboard the QuikSCAT satellite, which infers surface wind speed and direction. Launched in 1999, this scatterometer has encouraged various studies regarding early identification of tropical disturbances (Liu et al. 2001; Katsaros et al. 2001; Sharp et al. 2002). These studies, though operational in intent, hypothesized the potential for SeaWinds data to be applied towards research applications (i.e., genesis stage research). The main goal of this study is to develop an objective technique that will detect the early stages of TCG in the Atlantic basin using SeaWinds data.

Liu et al. (2001), Katsaros et al. (2001), and Sharp et al. (2002) demonstrated the ability to identify tropical disturbances, discrete weather systems of apparently organized convection that maintain their identity for 24 hours or more and are too weak to be classified as tropical cyclones (i.e., tropical depressions, tropical storms, or hurricanes), by the National Hurricane Center (NHC). Each technique utilized surface wind data obtained by the SeaWinds scatterometer. However, the criteria that defined their identification method differed. Sharp et al. (2002) employed vorticity in their detection condition, whereas Liu et al. (2001) and Katsaros et al. (2001) relied upon closed circulations apparent in the scatterometer data. Using a threshold of vorticity over a defined area, Sharp et al. (2002) identified numerous tropical disturbances and assessed whether or not they were likely to develop into tropical cyclones. Detection was based on surface structure, requiring sufficiently strong vorticity averaged over a large surface area. Unlike Sharp et al. (2002), Katsaros et al. (2001) and Liu et al. (2001) concentrated on disturbances that would develop into classified tropical cyclones. They examined surface wind patterns and looked for areas of closed circulation, successfully detecting tropical disturbances before designation as depressions. These studies illustrated the usefulness of SeaWinds data towards tropical disturbance detection, with the intent of improving operational activities. The early identification of surface circulations presented in these studies suggests an opportunity to detect the early stages of TCG, setting the basis for this paper.

The detection technique described herein has the potential for applications in the scientific and operational communities. In operational applications, the forecasting community can implement the detection technique as an additional observational tool. In doing so, the technique can enhance the current observing system employed to identify and monitor tropical weather systems, thereby reducing the time forecasters spend examining the tropics for incipient systems. In research applications, identification of the early stages of TCG can enhance understanding in regions where little research has been conducted due to the lack of surface observations, prior inability to conclusively locate TC precursor disturbances, and consequently the lack of observation studies (Reasor et al. 2005) on the establishment of the initial surface vortex. This study focuses on the Atlantic basin, but the detection technique can be applied to other tropical regions, such as the Pacific basin, after adjusting the threshold values to account for regional differences in TCG mechanisms.

The ability to detect the early stages of TCG provides an opportunity to classify tropical disturbances in the Atlantic basin based on the source of initial surface cyclonic vorticity.

Corresponding Author address: Mark A. Bourassa Center for Ocean-Atmospheric Prediction Studies, Florida State University, Tallahassee, FL 32306-2840. Email: bourassa@coaps.fsu.edu Phone: (850) 644-6923

Following categorization by Bracken and Bosart (2000) these sources include disturbances associated with: (i) monsoon troughs or the intertropical convergence zone (Riehl 1954, 1979), (ii) an easterly wave (Carlson 1969; Burpee 1972, 1974, 1975; Reed et al. 1977; Thorncroft and Hoskins 1994 ab), (iii) a stagnant frontal zone originating in the midlatitudes (Frank 1988; Davis and Bosart 2001), (iv) mesoscale convective systems (MCSs; Bosart and Sanders 1981; Ritchie and Holland 1997; Simpson et al. 1997; Bister and Emanuel 1997; Montgomery and Enagonio 1998), and (v) upper-level cut-off lows that penetrate to lower levels (Avila and Rappaport 1996). Among these, our research in the Atlantic basin affords the possibility to investigate cases associated with easterly waves. Of great interest is the prospect to examine the connection between a cold-core wave disturbance in the tropical easterlies and a warm-core tropical cyclone, which remains an unresolved issue in TCG research. Easterly waves are of great importance since approximately 63% of tropical cyclones in the Atlantic basin originate from African easterly waves (Avila and Pasch 1992).

Another fundamental issue with TCG involves the formation of the surface vortex prior to the onset of the Wind Induced Surface Heat Exchange (WISHE) intensification mechanism of Rotunno and Emanuel (1987). The generation of surface vorticity and its interaction within regions of deep cumulonimbus convection has been hypothesized in recent numerical (Hendricks et al. 2004; Montgomery et al. 2006) and observational (Reasor et al. 2005) studies to lead to the establishment of the initial surface vortex. The fine details of this surface vorticity organization process cannot be resolved with SeaWinds data. However, SeaWinds data may resolve the general evolution of vorticity and provide estimates of vorticity available at the surface prior to TCG, which are needed for numerical model initialization and validation.

2. DATA

Ocean wind vectors are obtained from the SeaWinds scatterometer for the Atlantic basin. QuikSCAT has slightly less than twice-daily coverage over this area and, hence, provides infrequent temporal sampling. To provide continuity of the track and verification of tropical disturbances between the relatively sparse QuikSCAT overpasses, GOES infrared images are acquired and compiled into animations. These animations allow cloud features that are associated with the surface vorticity signatures to be tracked. The conjunction of QuikSCAT and GOES is discussed in more detail in section 3.3.

2.1 *Scatterometer Data*

The scatterometer data that is used in this study is the simplified Ku2001 dataset produced by Florida State University's Center for Ocean-Atmospheric Prediction Studies (COAPS). It contains wind vectors, rain flags, locations, and times. The geophysical model function (GMF) used to obtain this data is the Ku2001 product developed by Remote Sensing Systems (RSS). The Ku2001 product is currently the most accurate GMF for most meteorological conditions (Bourassa et al. 2003). It performs far better near nadir, swath edges, and rain than either the science quality product from Jet Propulsion Laboratory (JPL) or the near real-time product from NOAA/NESDIS. This improved vector wind retrieval algorithm provides a fully integrated stand-alone rain flag and the capability to retrieve winds up to 70 m/s (Wentz et al. 2001). The scatterometer winds are calibrated to equivalent neutral winds at a height of 10 meters above the local mean water surface (Bourassa et al. 2003).

2.2 *GOES Imagery*

GOES-8 and GOES-12 infrared images are obtained from the NOAA/NESDIS Comprehensive Large Array-data Stewardship System (CLASS) for our 15 tropical cyclone cases during the 1999-2004 Atlantic hurricane seasons. Images are acquired approximately every three hours and compiled into separate animations, with a backward and forward-in-time progression.

3. METHODOLOGY

3.1 *Detection Technique*

The vorticity-based detection technique used in this study is a variation of the method developed by Sharp et al. (2002). This technique calculates relative vorticity within the SeaWinds swaths and applies a mean vorticity threshold over a specified spatial area (Sharp et al. 2002). Different criteria are utilized than those of Sharp et al. (2002), permitting earlier identification of tropical disturbances.

The spatial scale for averaging vorticity within the SeaWinds swaths is a 100 km by 100 km area. Individual vorticity values are calculated from wind observations, defined by 4 [2 x 2] adjacent scatterometer vectors, by determining the circulation around each box and then dividing through by the area (Sharp et al. 2002). This

method enables the vorticity to be calculated at the same spatial density as the wind observations. In each calculation a minimum of 3 wind vectors out of the 4 in a square are required (if only 3 wind vectors exist, the square becomes a triangle). The wind vector data we use in this approach includes rain-flagged data, which are prone to ambiguity removal errors (reversal of wind direction). Incorporation of rain-flagged data can affect the vorticity calculation, resulting in noise. How this noise compares to the signal varies across the QuikSCAT vorticity-based track of tropical disturbances and is discussed in section 5.

The criteria that define the detection technique consist of three components. These criterion require that at the specified spatial scale (100 km by 100 km area): the average vorticity must exceed a minimum vorticity threshold, and the maximum rain-free wind speed must exceed a minimum wind speed threshold. The third criterion is that these conditions be met for at least 80% of the overlapping 100 by 100 km boxes centered on the vorticity points within 50 km of the vorticity points being tested. If these criteria are met, then the system under consideration is deemed a tropical disturbance, which may develop into a tropical cyclone. For this study, the 15 cases chosen are classified tropical cyclones and, hence, are known to develop. The thresholds used here are greatly reduced from those of Sharp et al. (2002).

3.2 *Threshold Determination*

The threshold values defined in our detection technique are determined using research-quality SeaWinds data for 15 tropical cyclones during the 1999-2004 Atlantic hurricane seasons. In preliminary examples we applied a speed and vorticity threshold of 4.0 ms^{-1} and $2.0x10^{-5}$ s^{-1}, respectively. Results showed that 65 wind fields sampled by the overpasses fit these criteria; however, some of the vorticity signatures identified were indistinguishable from noise (i.e., false alarms). Therefore, it was determined that these threshold values were too small. To reduce the number of false alarms found in our preliminary example, a categorical score is computed for a range of vorticity and wind speed thresholds to determine appropriate values.

The categorical score considered in this study is the probability of detection (POD), which evaluates the effectiveness of detection techniques. It is defined as:

$$POD = \frac{H}{H + M} \qquad (1)$$

where H is the number of hits and M is the number of misses. Using the GOES imagery, the cloud cluster broadly associated with each of the 15 classified tropical cyclones is traced back in time. In QuikSCAT overpasses, a "hit" is a vorticity signature that fulfills the detection technique's criteria within close proximity (175 km) to the identified relevant cloud cluster center, and a "miss" is a vorticity signal that does not meet the detection technique's criteria within this close proximity. The POD score measures the ability of our technique to accurately identify tropical disturbances in the correct locations. A score of 1 indicates perfect detection (all vorticity signatures in the QuikSCAT overpasses are hits), whereas, a score of zero represents negligible detection (all vorticity signatures in the QuikSCAT overpasses are misses).

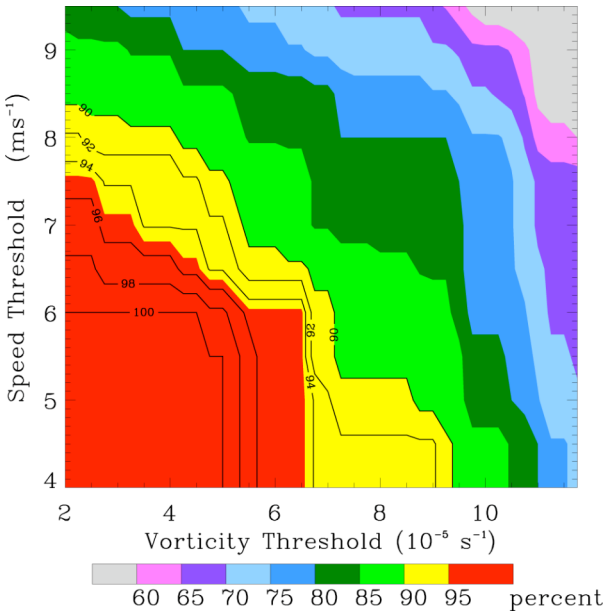

Figure 1. Probability of Detection (POD) graph. Lower threshold values result in a higher probability of detection and increased false alarms. Higher threshold values result in detection of stronger systems (more misses) and, hence, less false alarms.

In order to examine this method, a POD plot is produced that assesses the contributions from both wind speed and vorticity thresholds in regards to our preliminary example (Fig. 1). This plot illustrates that low threshold values result in a higher probability of detection (albeit more false alarms), whereas, high thresholds result in a lower probability of detection. A POD score of 1 is most desirable since it represents perfect detection;

however, the test cases include two examples that are indistinguishable from noise. Through analysis, the 96% POD contour is chosen based on its large gradient and high sensitivity area, as well as its reduction of false alarms. Threshold values associated with this contour include a vorticity and wind speed threshold of 5.0×10^{-5} s^{-1} and 6.3 ms^{-1}, respectively. Utilization of these values within our detection technique shows that 62 wind fields sampled by the overpasses meet our criteria.

3.3 *Track Assessment*

The combination of QuikSCAT's four-day repeat cycle and approximate twice-daily coverage (globally averaged) affords the Atlantic basin with infrequent temporal samplings, which proves problematic in regards to studies based purely on QuikSCAT. As previously mentioned, 62 QuikSCAT overpasses contain tropical disturbances that fulfill the detection technique's criteria. Though substantial in number, the time period between these overpasses is anything but adequate, with a range from 11 to 36 hours. These temporal gaps may not be a problem for detection of existing tropical cyclones or tropical disturbances near classification; however, they are significant for identification of tropical disturbances associated with the early stages of TCG. Gaps between detection generate uncertainty regarding a tropical disturbance's track and positioning in time. To provide continuity of the track, which is used to validate the vorticity signatures identified by the detection technique, the combination of GOES and QuikSCAT is necessary.

GOES infrared images provide supplementary observational guidance between the relatively sparse QuikSCAT overpasses. For the 15 cases, GOES animations are created with a backward and forward-in-time progression. These animations allow the cloud mass associated with a tropical disturbance to be tracked, providing insight into the position and track extent of the tropical disturbance. For a large, organized cloud mass, the location of the corresponding surface vorticity signature is evident within QuikSCAT-derived relative vorticity swaths. However, through the pre-tropical cyclone tracks of our 15 cases, it is apparent that the cloud masses go through phases of intensification and de-intensification (i.e., maturing and dissipating cloud masses). Categorization of these phases is dependent upon spatial size, organization, and convective features. If the cloud mass associated with a tropical disturbance is going through de-intensification it may separate into numerous cloud clusters, making it difficult to pinpoint a specific cloud cluster and, hence, a position to use in testing the detection algorithm. The use of QuikSCAT and GOES together greatly reduces the ambiguity in determining which cloud system to track.

4. RESULTS

Results for the 15 tropical cyclones during the 1999-2004 Atlantic hurricane seasons are listed in Table 1. These systems are chosen because their coverage is adequate for reasonable study in the Atlantic basin. Ten of the 15 tropical cyclones originate as tropical waves off the coast of Africa (i.e., African easterly waves). These include Floyd (1999), Debby (2000), Nadine (2000), Jerry (2001), Dolly (2002), Danny (2003), Isabel (2003), Juan (2003), Nicholas (2003), and Alex (2004). The other five cases originate from sources other than tropical waves, such as upper-level cut-off lows and stagnant frontal zones. These include Florence (2000), Michael (2000), Karen (2001), Noel (2001), and Gustav (2002).

Table 1. Results for 15 tropical cyclones during the 1999-2004 Atlantic hurricane seasons. The last column signifies the hours elapsed between the NHC initial classification and our earliest tropical disturbance identification (i.e., tracking time).

Storm	Year	NHC Initial Classification	Tracking Time
Floyd	1999	Tropical Depression	46
Debby	2000	Tropical Depression	95
Florence	2000	Subtropical Depression	67
Michael	2000	Subtropical Depression	38
Nadine	2000	Tropical Depression	50
Jerry	2001	Tropical Depression	101
Karen	2001	Extratropical Low	19
Noel	2001	Subtropical Storm	62
Dolly	2002	Tropical Depression	53
Gustav	2002	Subtropical Depression	25
Danny	2003	Tropical Depression	38
Isabel	2003	Tropical Depression	101

Juan	2003	Tropical Depression	26
Nicholas	2003	Tropical Depression	64
Alex	2004	Tropical Depression	79

Tropical disturbances associated with the early stages of TCG are found for these cases within a range of 19 hours to 101 hours before classification as tropical cyclones by the NHC (Table 1). The average tracking time for these systems is approximately 58 hours, where tracking time is defined as the time elapsed between the NHC initial classification and our earliest tropical disturbance identification. Some examples of the technique in identifying the early stages of TCG are illustrated in Figs. 2 and 3. These figures show QuikSCAT-derived relative vorticity overlaid with solid black contours, signifying the locations where the detection technique's criteria are met within 175 km from the cloud cluster center in the associated GOES infrared image. Though we have cases for a variety of sources, primary focus centers on those cases associated with easterly waves. These cases are chosen due to the ability of our detection technique to track the tropical disturbances associated with these tropical cyclones back to the coast of Africa where they originate as easterly waves.

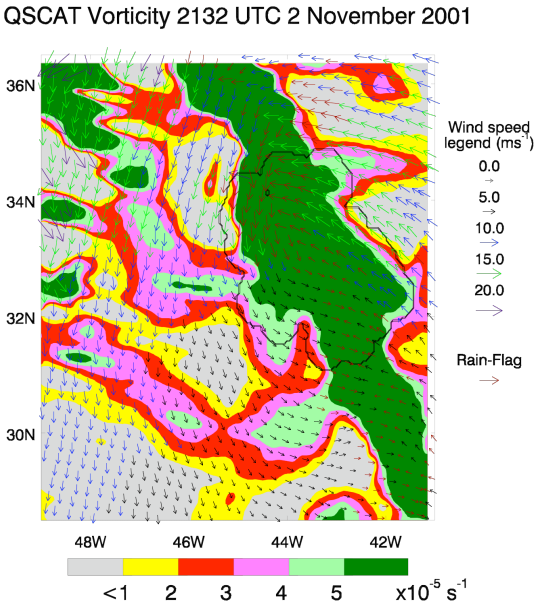

Figure 2. Noel, 26 hours before classification as a subtropical storm. The vorticity signature shown is associated with the non-tropical occluded low that produces Noel.

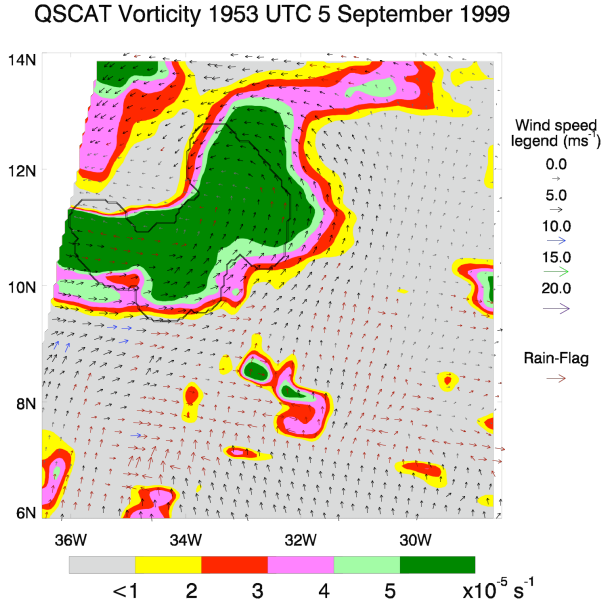

Figure 3. Floyd, 46 hours before classification as a tropical depression. The vorticity signature shown is associated with the easterly wave that spawns Floyd.

The transition from an easterly wave to tropical cyclone is clearly evident in the pre-tropical cyclone (pre-TC) tracks of the easterly wave cases. This evolution is depicted through comparison of the wind and rain signatures in the areas where the detection technique's criteria are fulfilled within 175 km from the cloud cluster center. Based upon the relationship between the wind and rain signatures, the evolution is subdivided into stages (section 5).

5. DISCUSSIONS

Results from the vorticity-based detection technique prove very effective in identification of tropical disturbances; however, the principal concern with this technique regards the ambiguity removal errors associated with rain-flagged data. These selection errors are evident for the majority of the 15 cases, but the cases more seriously affected are those originating in the tropics (i.e., easterly waves). Disturbances connected with this origin exhibit lower wind speeds and high moisture content, contributing to the significant number of rain flags and, hence, ambiguity removal errors. In contrast, cases that develop from sources other than tropical waves, such as upper-level cut-off lows and stagnant frontal zones, are generally unaffected by the negative influences of rain (i.e.,

selection errors). Systems associated with such sources have subtropical origins and therefore exhibit higher wind speeds and reduced moisture content. A key example of a subtropical system that illustrates such features is the disturbance associated with pre-TC Noel on November 2 (Fig. 2).

Incorporation of these selection errors within the technique significantly impacts the vorticity calculation. As previously mentioned, average vorticity is calculated within a 100 km by 100 km area using individual vorticity values, which are determined from wind observations via the circulation theorem (section 3.1). Therefore, if the wind observations used to calculate vorticity at each grid cell include ambiguity removal errors on the outer bounds of the spatial domain, then the average vorticity is affected. The location where these selection errors (i.e., incorrectly selected ambiguities) influence the averaged vorticity is approximately 100 to 140 km from the selection errors.

Cases associated with easterly waves can be considerably affected by the ambiguity selection errors associated with rain-flagged data. The rain-related issues in these two case studies vary throughout the QuikSCAT vorticity-based track; however, a similar vorticity signal-to-noise pattern is evident through comparison of the wind and rain signatures (associated with vorticity signatures that met the detection technique's criteria within 175 km from the cloud cluster center). The relationship between these signals (i.e., wind speed and rain) has been previously characterized (Weissman et al. 2002).

The amount of backscattered power that is received by the scatterometer is a function of wind speed and rain characteristics (Weissman et al. 2002). If the wind signal is larger than that of the rain signal, then rain insignificantly affects the backscatter signal. However, if the rain signal is larger than that of the wind signal, then rain influences the backscattered power. The influence of rain distorts the scatterometer signal, potentially creating wind direction reversals in the data which affect the average vorticity calculation. In areas strongly dominated by rain, the scatterometer directions are perpendicular to the nadir track.

Based upon the relationship between wind and rain signatures in the areas where the detection technique's criteria are met (within 175 km from the cloud cluster center), the pre-TC tracks of each easterly wave case are subdivided into stages. These stages consist of an initial, intermediate, and near-TC phase. The initial stage corresponds to the earliest vorticity signatures identified by the detection technique, the near-TC stage is associated with the vorticity signatures detected directly prior to NHC classification, and the intermediate stage constitutes the vorticity signatures between the initial and near-TC stages. Each of these phases is discussed in detail in subsequent sections (sections 5.1-5.3). These stages depict the transition of a tropical disturbance within an easterly wave to a tropical cyclone, and are further discussed in section 5.4.

5.1 The Initial Stage

The vorticity signatures that are identified by the detection technique are small in spatial extent and very weak. These initial vorticity signatures correspond with rain-flagged wind vectors and few large ambiguity removal errors (i.e., wind direction reversals). This situation implies that the wind signal is larger than the rain signal (Weissman et al. 2002). Therefore, any vorticity modification that occurs as a result of selection errors is small when compared to the signal.

5.2 The Intermediate Stage

Relative to the initial stage, the vorticity signatures identified in the intermediate stage are stronger and have a larger spatial size. The areas where the detection technique's criteria are fulfilled (black solid contours) are inundated with numerous rain-flagged wind vectors and ambiguity removal errors, implying that the vertically integrated rain rates have increased relative to the initial stage. The rain-flagged wind vectors are comparatively large in magnitude and exhibit an across swath direction, signifying rain contamination. This situation implies that the rain signal has grown to dominate the wind signal. Medium to strong tropical storms also have this characteristic. Thus, rain-related vorticity modification is equivalent or large when compared to the signal. In these instances, several of the detected location areas appear to be a result of ambiguity selection errors. In regards to this stage, the detection technique is pinning down the general area of the tropical disturbance and, though some identified signatures are byproducts of selection errors, the detection technique is effective. In general, the intermediate stage is the development phase of the pre-TC tracks. Reasoning behind this stems from the beginning of a cyclonic circulation in the surrounding wind pattern and increase of vertically integrated rain rates.

5.3 The Near-TC Stage

Vorticity signatures associated with the near-TC stage are approximately one to two days prior to NHC classification. These signatures are very organized and have a large spatial size. A large-scale cyclonic circulation is present for each signature with strong wind speeds (strong in relation to the wind speeds in the initial and intermediate stages). The near-TC vorticity signatures correspond with rain-flagged wind vectors and few ambiguity removal errors. This situation implies the wind signal dominates the rain signal. Therefore, any vorticity modification that occurs as a result of selection errors is small when compared to the signal. Relative to the intermediate stage, the near-TC stage, with less rain-related problems, indicates that either the rain rate has been reduced (which we have not examined) or that the wind speeds have increased, the latter of which appears to be true.

5.4 Pre-TC Track Transition

The vorticity signal-to-noise pattern associated with the QuikSCAT vorticity-based tracks of the easterly wave cases clearly depict the transition of a tropical disturbance within an easterly wave to a tropical cyclone and the phases associated with this transition (initial, intermediate, and near-TC stage). The initial stage is associated with very weak vorticity signatures that have small spatial scales. These initial signals are often related to horizontal shear embedded in eastward winds and are insignificantly affected by rain. The intermediate stage constitutes vorticity signatures that are greatly influenced by rain and rain-related problems, as well as the beginning of a large-scale cyclonic circulation. The intermediate stage is of significant importance to the evolution of a tropical disturbance within an easterly wave to a tropical cyclone since it represents a development stage. As a result of this growth, the vorticity signatures corresponding to the near-TC stage are highly organized, with large spatial sizes, increased wind speeds, and large-scale cyclonic circulations. The surface signatures of these tropical disturbances, as well as the cloud pattern, continue to strengthen and organize.

6. CONCLUSIONS

A vorticity-based detection technique is developed to identify and monitor tropical disturbances associated with the early stages of TCG in the Atlantic basin. Calibration of the detection technique is based on visual inspection of GOES infrared images, as well as surface structure. Herein, only disturbances that grew into tropical cyclones were examined. From a sampling of 15 tropical cyclones during the 1999-2004 Atlantic hurricane seasons, the technique identifies tropical disturbances approximately 19 to 101 hours before classification by the NHC. Herein the minimum tracking time is associated with pre-TC Karen (2001); whereas, the maximum tracking time is associated with pre-TC Jerry (2001) and pre-TC Isabel (2003). Smaller tracking times are associated with systems that develop from sources other than easterly waves, such as upper-level cut-off lows and stagnant frontal zones. The shorter tracking times stem from land interference, which QuikSCAT lacks the ability to resolve since it only provides observations over water. Larger tracking times correspond to cases that originate from African easterly waves. Focus is primarily concentrated on such cases, due to approximately 63% of all Atlantic tropical cyclones being associated with tropical waves.

Overall results for the 15 cases prove very successful. Therefore, the vorticity-based detection technique described herein is an effective tool in identifying and monitoring tropical disturbances in the genesis stage. For easterly wave cases, the detection technique has the ability to track tropical disturbances from near the coast of Africa. The pre-TC tracks of these cases depict the evolution of a tropical disturbance within an easterly wave to a tropical cyclone and stages associated with this transition. These stages consist of an initial, intermediate, and near-TC phase, which are related to spatial extent, wind speed, and precipitation characteristics. Though there is room for improvements regarding scatterometer design and wind retrieval algorithms to better account for the influences of rain, it is reasonable to assume that this technique could be useful to scientific and operational communities.

Acknowledgments. Support for the scatterometer research came from the NASA/OSU SeaWinds project and the NASA OVWST project. QuikSCAT data are produced by Remote Sensing Systems and sponsored by the NASA OVWST. Data are available at www.remss.com. GOES images are provided by NOAA/NESDIS/CLASS and are available at www.class.noaa.gov. COAPS receives base funding NOAA CDEP.

REFERENCES

Avila, L. A., and R. Pasch, 1992: Atlantic tropical systems of 1991. *Mon. Wea. Rev.,* **120**, 2699-2696.

Avila, L. A., and E. N. Rappaport, 1996: Atlantic hurricane season of 1994. *Mon. Wea. Rev.,* **124**, 1558-1578.

Bister, M., and K. A. Emanuel, 1997: The genesis of Hurricane Guillermo: TEMEX analyses and a modeling study. *Mon. Wea. Rev*., **125**, 2662-2682.

Bosart, L. F., and F. Sanders, 1981: The Johnstown flood of July 1977: A long-lived convective system. *J. Atmos. Sci.,* **119**, 1979-2013.

Bourassa, M. A., D. M. Legler, and J. J. O'Brien, 2003: Scatterometry Data Sets: High Quality Winds Over Water. *Advances in the Applications of Marine Climatology – The Dynamic Part of the WMO Guide to the Applications of Marine Climatology*. JCOMM Technical Report No. 13 WMO/TD-No.1081, 159-174.

Bracken, W. E., and L. F. Bosart, 2000: The role of synoptic scale flow during tropical cyclogenesis over the North Atlantic Ocean. *Mon. Wea. Rev.,* **128**, 353-376.

Burpee, R. W., 1972: The origin and structure of easterly waves in the lower troposphere in North Africa. *J. Atmos. Sci.,* **29**, 77-90.

Burpee, R. W., 1974: Characteristics of North African easterly waves during the summers of 1968 and 1969. *J. Atmos. Sci.,* **31**, 1556-1570.

Burpee, R. W., 1975: Some features of synoptic-scale waves based on compositing analysis of GATE data. *Mon. Wea. Rev.,* **103**, 921-925.

Carlson, T. N., 1969: Synoptic histories of three African wave disturbances that developed into Atlantic hurricanes. *Mon. Wea. Rev.,* **97**, 921-925.

Davis, C. A., and L. F. Bosart, 2001: Numerical simulations of the genesis of Hurricane Diana (1984). Part I: Control simulation. *Mon. Wea. Rev.,* **129**, 1859-1881.

Frank, W. M., 1988: Tropical cyclone formation. *A Global View of Tropical Cyclones*, R.L. Elsberry, Ed., 53-90.

Hendricks, E. A., M. T. Montgomery, and C. A. Davis, 2004: On the role of "vortical" hot towers in formation of tropical cyclone Diana (1984). *J. Atmos. Sci.,* **61**, 1209–1232.

Katsaros, K. B., E. B. Forde, P. Chang, and W. T. Liu, 2001: QuikSCAT's SeaWinds facilitates early identification of tropical depressions in 1999 hurricane season. *Geophys. Res. Lett*., **28**, 1043-1046.

Liu, W. T., 2001: Wind over troubled water. *Backscatter*, **12**, 10-14.

Montgomery, M. T., and J. Enagonio, 1998: Tropical cyclogenesis via convectively forced vortex Rossby waves in a three-dimensional quasigeostrophic model. *J. Atmos. Sci.*, **55**, 3176-3207.

Montgomery, M. T., M. E. Nicholls, T. A. Cram, and A. B. Saunders, 2006: A vortical hot tower route to tropical cyclogenesis. *J. Atmos. Sci.,* **63**, 355–386.

Reasor, P. D., M. T. Montgomery, and L. Bosart, 2005: Mesoscale observations of the genesis of Hurricane Dolly (1996). *J. Atmos. Sci.,* **62**, 3151–3171.

Reed, R. J., D. C. Norquist, and E. E. Recker, 1977: The structure and properties of African wave disturbances as observed during Phase III of GATE. *Mon. Wea. Rev.,* **105**, 317-333.

Riehl, H., 1954: *Tropical Meteorology*. McGraw-Hill, 392 pp.

Riehl, H., 1979: *Climate and Weather in the Tropics*. Academic Press, 611 pp.

Ritchie, E. A., and G. H. Holland, 1997: Scale interactions during the formation of Typhoon Irving. *Mon. Wea. Rev.,* **125**, 1377-1396.

Rotunno, R., and K. A. Emanuel, 1987: An air–sea interaction theory for tropical cyclones. Part II: Evolutionary study using a nonhydrostatic axisymmetric numerical model. *J. Atmos. Sci*., **44**, 542–561.

Sharp, R. J., M. A. Bourassa, and J. J. O'Brien, 2002: Early detection of tropical cyclones using SeaWinds-derived vorticity. *Bull. Amer. Meteor. Soc*., **83**, 879-889.

Simpson, J., E. Ritchie, G. J. Holland, J. Halverson, and S. Stewart, 1997: Mesoscale interactions in tropical cyclone genesis. *Mon. Wea. Rev*., **125**, 2643-2661.

Thorncroft, C. D., and B. J. Hoskins, 1994a: An idealized study of African easterly waves. Part I: A linear view. *Quart. J. Roy. Meteor. Soc.,* **120**, 953-982.

Thorncroft, C. D., and B. J. Hoskins, 1994b: An idealized study of African easterly waves. Part II: A nonlinear view. *Quart. J. Roy. Meteor. Soc.,* **120**, 983-1015.

Weissman, D. E., M. A. Bourassa, and J. Tongue, 2002: Effects of rain rate and wind magnitude on SeaWinds scatterometer wind speed errors. *J. Atmos. Oceanic Technol.,* **19**, 738-746.

Wentz, F. J., D. K. Smith, C. A. Mears, and C. L. Gentemann, 2001: Advanced algorithms for QuikSCAT and SeaWinds/AMSR. *Geoscience and Remote Sensing Symposium, 2001. IGARSS'01. IEEE 2001 International, 3, 1079-1081.*